2D sound source localization technology based on diaphragm EFPI fiber microphone array

Sijun Zhang [a], Shengpeng Wan* [a], Yangfeng Wang [a], Bin Zhang [a], Zhengping Zhang [a], Haihua Zhong [a], Jiulin Shi [b], Jizhou Sun [b], Xingdao He [b], Qiang Wu [c]

[a] Key Laboratory of Nondestructive Testing (Nanchang Hangkong University), Ministry of Education, Nanchang Hangkong University, Nanchang 330063, China

[b] Key *Laboratory of Opto-Electronic Information Science and Technology of Jiangxi Province, Nanchang Hangkong University, Nanchang 330063, China*

[c] *Department of Mathematics, Physics and Electrical Engineering, Northumbria University, Newcastle Upon Tyne NE1 8ST, U.K.*

Keywords:
Diaphragm EFPI
positioning
Effective signal extraction
TDOA

ABSTRACT

The technologies of two-dimensional sound source localization based on diaphragm extrinsic Fabry-Perot interferometer (EFPI) fiber microphone array have been studied in this paper. The fiber microphone array consists of three EFPI. Self-calibrated intensity demodulation technology with simple structure and low cost is adopted to demodulate the sound signals. Using effective sound signal extraction technology to find the starting point and end point of sound signal, combining with time differences of arrival (TDOA) positioning technology, high-precision sound source location is successfully realized. The average positioning error of this system is no larger than 4.82%. The system has the advantages of low cost, high practicability and wide application scenarios.

1. Introduction

Fiber optical sensor has the characteristics of passive detection end, anti-electromagnetic interference, low loss, corrosion resistance and long distance [1]. Because it is free from electromagnetic interference and various new optical fiber materials (such as sapphire fiber and plastic fiber) appear, the optical fiber acoustic sensor is safe and reliable, and it can be used in high temperature, high pressure, strong radiation, strong electromagnetism and other environments where traditional electroacoustic sensors are difficult to work normally. Therefore, optical fiber acoustic sensors have received extensive attentions and applications in the field of national defense and security [2], oilfield monitoring [3], medical diagnosis [4], remote monitoring of gas micro-leakage [5], etc.. Comparing with other optical fiber acoustic sensors, the F-P sensors have obvious advantages in sensitivity, dynamic range and miniaturization [6].

Because the traditional electroacoustic sensors can't work in the harsh environment such as liquid nitrogen [7], the sound source localization technology based on optical fiber acoustic sensor has attracted extensive research interest in recent years [8-12]. In [8], three Fabry-Perot sensors are used to achieve a positioning accuracy of 3.55cm in the spatial range of 60cm×60cm. In [9], four Fabry-Perot sensors are used to achieve a positioning accuracy of 2.42cm in the spatial range of 30cm×30cm. In [10], in order to achieve 3D sound source localization, four Fabry Perot sensors array are used. The positioning accuracy of 3.45cm is realized in the spatial range of 100cm×100cm×100cm. In [11], five sensitive units used in phase-sensitive optical time domain reflectometry (φ-OTDR) to achieve a positioning accuracy of 3.4358cm in the spatial range of 50cm×40cm×30cm. Up to now, most multi-point optical fiber acoustic detection systems are based on fiber Bragg gating (FBG) sensor array [10], because they have multiplexing characteristics in wavelength domain. However FBG sensors cannot achieve high-frequency measurement and have problems such as complex demodulation, high demodulation cost and low sensitivity. Optical fiber EFPI acoustic sensor combining with high performance and flexible multipoint demodulation is more suitable for sound source location because of its advantages of probe structure, high sensitivity, simple

structure and low cost.

Intensity demodulation is one of the most widely used demodulation techniques for EFPI acoustic sensors [11], but it requires high quality of light source, high cost and low practicability. Phase demodulation schemes such as Phase Generated Carrier (PGC) demodulation have larger dynamic range and better stability, but it's demodulation method usually needs piezoelectric ceramic transducer (PZT) to generate phase carrier, which will make the system bulky. Furthermore, the mechanical properties of PZT will lead to a limited frequency response range [12]. However, self-calibrated intensity demodulation only needs broadband light source to demodulate signals [13], which has the characteristics of low cost, strong practicability and wide application scenarios.

In this paper, self-calibrated intensity demodulation system is adopted to test the performance of fiber microphone. Experimental results demonstrated that the system has good performance in stability, sensitivity and dynamic range. Moreover, we establish an optical fiber localization system based on cross-correlation algorithm and realize the sound source localization in two-dimensional plane by only using three optical microphones. The positioning system has the characteristics of simple structure, high positioning accuracy and low cost.

2. **Fabrication process and positioning principle of optical fiber microphone**

2.1. Fabrication and performance test of optical fiber microphone

The manufacturing process of EFPI fiber microphone is shown in Fig.1. First, as shown in Fig.1 (a), the ferrule is bonded to one end of a glass sleeve with an inner diameter of 3mm with ultraviolet glue, and then irradiated and cured under ultraviolet light; Secondly, as shown in Fig.1 (b), adhere the manufactured Graphene Oxide(GO) diaphragm to the other end of the glass tube.

The process of fabricating GO diaphragm is similar to the method in [14]. The manufacturing process of GO diaphragm in this paper is shown as follows:

(1) Put the GO solution with the concentration of 200mg/L into the ultrasonic cleaner and shake it for 4-5 times, 20 minutes each time, with an interval of 10 minutes each time. This step is to make the GO solution more uniform, so that the prepared GO film is more stable and not easy to disperse;

(2) Use the rubber head dropper cleaned with deionized water to draw an appropriate amount of prepared GO solution and drop it on the surface of 1×1cm square copper foil with a thickness of 0.05mm, let it dry naturally at room temperature;

(3) After the water evaporates, a circle of light colored GO film will be formed on the copper foil. Cut the copper foil into a square of appropriate size and place it in the corrosion solution prepared by environmental protection etchant. After the copper foil is completely corroded, the GO film will suspend above the liquid level. Finally, use glass to transfer the prepared GO film to deionized water for cleaning.

So far, the whole preparation process of GO film is over.

The thinner the GO diaphragm, the higher the sensitivity of the fabricated sensor.

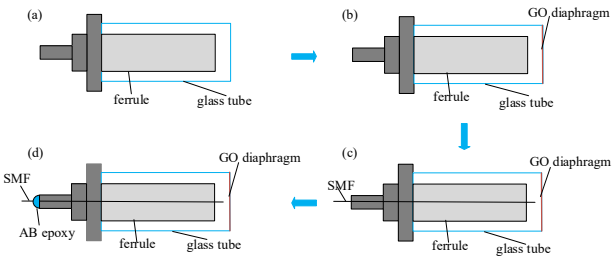

Fig.1. Fabrication of EFPI fiber optic microphone.

Then, as shown in Fig.1 (c), the optical fiber (SMF) is inserted into the ceramic ferrule, the distance between the fiber end face and the GO diaphragm is controlled by three-dimensional moving stage to form a microcavity structure. At the same time, the system shown in Fig.2 can be used to calibrate the initial cavity length.

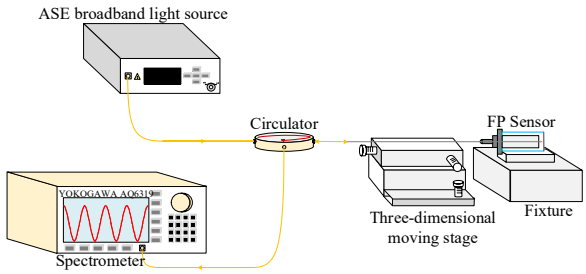

Fig. 2. Cavity length calibration system of EFPI acoustic sensor.

In the process of moving the three-dimensional moving stage, with the change of cavity length, the spectrum observed on the spectrometer also changes. It can be considered that the initial cavity length of the optical fiber microphone has been found when the fringe contrast of the interference spectrum is greater than 15dB. The interference spectrum of the sensor in this paper is shown in Fig.3.

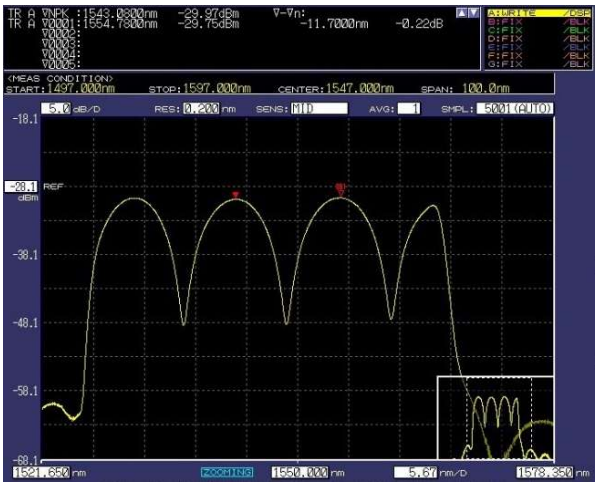

Fig. 3. Interference spectrum of EFPI acoustic sensor.

It can be seen from the interference spectrum that the interference fringe contrast of the sensor is about 18dB. The wavelengths of two adjacent peaks are $\lambda_1 = 1543.08\text{nm}$ and $\lambda_2 = 1554.78\text{nm}$, respectively. According to the fringe counting method, the cavity length can be obtained as follows

$$L = \frac{\lambda_n \lambda_{n+1}}{2(\lambda_n - \lambda_{n+1})} \tag{1}$$

By substituting λ_1 and λ_2 into (1), we can obtain the cavity length of the acoustic sensor $L = 102.528\mu\text{m}$.

Finally, as shown in Fig.1 (d), the sensor has been successfully manufactured after the sensor is encapsulated with AB epoxy.

The fiber microphone self-calibrated intensity demodulation system is shown in Fig.4. The light coming from the broadband light source is launched into the EFPI fiber microphone through the first circulator, and then the reflected light enters the fiber Bragg grating (FBG) through the second circulator. The Bragg wavelength of the fiber Bragg grating is located at the midpoint of the linear region of the interference spectrum of the EFPI sensor head. As shown in Fig.5, the linear region of EFPI sensor head is around 1550nm, so we chose FBG with center wavelength of 1550nm, 3dB bandwidth of 0.2nm and reflectivity greater than 90%. After passing through the second circulator, The signal light I_R reflected from the FBG is received by photo-detector 1(PD1). The reference light I_T transmitted from the FBG is received by PD2. The analog-to-digital converter (ADC) module is used to collect two voltage signals after photoelectric conversion, and the collected data is transmitted to PC terminal for processing through field-programmable gate array (FPGA) development board.

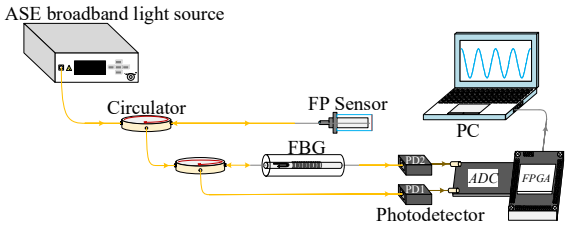

Fig.4. Self-calibrated intensity demodulation system.

I_R contains not only the signal to be measured, but also the noise such as light source intensity noise and optical fiber disturbance noise. However, I_T contains only the noise, such as light source intensity noise and optical fiber disturbance noise. Therefore, taking the normalized value of the I_T as the self-calibrated coefficient C, the reflected light intensity after compensation can be expressed as [15]

$$\overline{I_{selfcal}} = \frac{I_R}{C} \tag{2}$$

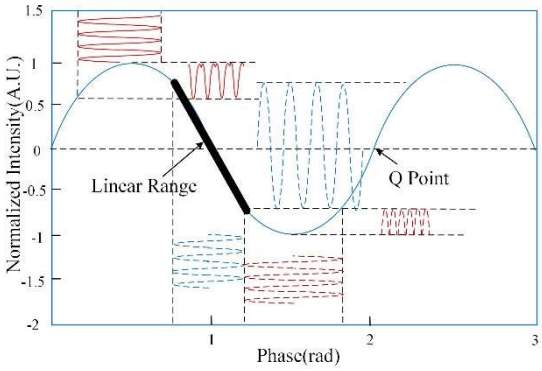

Fig.5. Working point Q.

2.2. Sound source localization model based on TDOA

The structure of the fiber microphone array used in this paper are shown in Fig.6 and the sound source localization model based on TDOA is adopted.

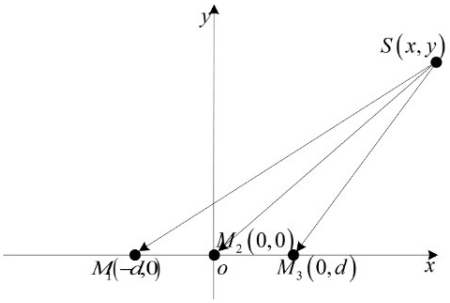

Fig. 6. Linear fiber microphone array for sound source localization.

For the array composed of three fiber microphones, the received signal $x_i(t)$ of the *i-th* $(i = 1,2,3)$ optical fiber microphone M_i can be expressed as

$$x_i(t) = \alpha_i s(t - \tau_i) + n_i(t) \tag{3}$$

Where α_i represents the propagation attenuation factor of the sound source $s(t)$, which is inversely proportional to the square of the propagation distance. τ_i represents the delay of the sound source $s(t)$ reaching the optical fiber microphone M_i, and $n_i(t)$ represents the additive white

noise received by the optical fiber microphone M_i. Then the cross-correlation function of the signals received by the *i-th* and *j-th* optical fiber microphones can be expressed as

$$R_{x_i x_j}(\tau) = E\left[x_i(t)x_j(t-\tau)\right] \tag{4}$$

Based on (3), (4) can be written as:

$$R_{x_i x_j}(\tau) = E\{[\alpha_i s(t-\tau_i) + n_i(t)]\left[\alpha_j s\left(t-\tau_j\right) + n_j(t)\right]\} \tag{5}$$

The TDOA between the M_i and M_j microphone can be expressed as τ_{ij}, and the autocorrelation function of the sound signal is expressed by $R_S(\tau_{ij})$. Because there is no correlation between noise and noise, sound source and noise, the cross-correlation function between $x_i(t)$ and $x_j(t)$ can be written as

$$R_{x_i x_j}(\tau) = \alpha_i \alpha_j R_S\left(t - \tau_{ij}\right) \tag{6}$$

When the cross-correlation function takes the maximum value, $t - \tau_{ij} = 0$. Therefore, we can obtain the time difference τ_{ij} by searching the position where the maximum value of the cross-correlation function of the two signals is located.

The most critical step is to judge the starting and ending positions of the acoustic signal in the process of accurately obtaining τ_{ij}. We use $x_{ij}(t)$ as a discrimination signal, where $x_{ij}(t)$ is composed of two signals $x_i(t)$ and $x_j(t)$ received by sensor M_i and sensor M_j, signal $x_i(t)$ is the odd term of $x_{ij}(t)$, and signal $x_j(t)$ is the even term of $x_{ij}(t)$. The variance feature is used to divide the whole signal $x_{ij}(t)$ into k segments, N sampling points in each segment, calculate the signal variance of each segment, and take the median of these k variances as the threshold to find the starting and ending points of the sound. Generally, the curve in the neighborhood of the starting and ending points is relatively steep, and the variance of nearby signal segments is relatively large. In the whole signal, the variance of the non-voiced signal segment is the smallest, and taking the median as the threshold can more keenly perceive the sudden change of the signal. After the threshold is set, a sliding window is executed at both ends of the whole section of signal respectively. The length of the window is N and 10 sampling points are slid each time. When the variance of the signal in the sliding window exceeds the threshold at a certain moment, it is considered that the critical point of starting or ending has been found.

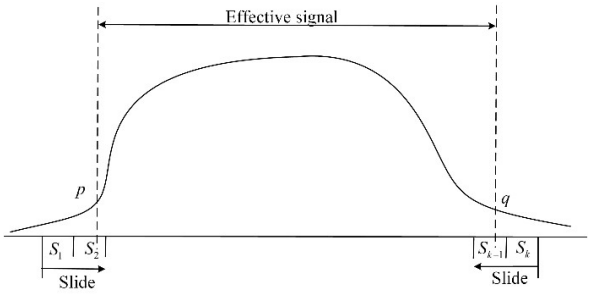

Fig. 7. Effective signal extraction.

The position of sound source is calculated by geometric positioning technology after obtaining the estimated value of time delay [17].

A rectangular coordinate system is established using M_2 as the reference array element in Fig.6. The coordinate of sound source S is (x, y), τ_{12} is the TDOA between sensor M_1 and sensor M_2, τ_{23} is the TDOA between sensor M_2 and sensor M_3. Based on the distance difference, geometric positioning technology can be expressed as

$$\begin{cases} \sqrt{(x+d)^2 + y^2} - \sqrt{x^2 + y^2} = v\tau_{12} \\ \sqrt{x^2 + y^2} - \sqrt{(x-d)^2 + y^2} = v\tau_{23} \end{cases} \tag{7}$$

Where $v = 346.8662m/s$ is the sound velocity in the air. The intersection of two semi-hyperbolas can be obtained by solving (7), which is the possible sound source position. Finally, the actual position coordinates can be judged from the starting point and the end point of the sound.

3. Experimental results and discussion

We established a self-calibrated intensity demodulation system to demonstrate the validity and performance of the fiber-optic microphone. We seting the FPGA sampling rate to 11025Hz and collecting a section of 30s audio data. The sound waveform after compensation is shown in Fig.8. Fig.8 shows that the noise of the acoustic signal after wavelet transform algorithm is very small and the signal-to-noise ratio is very high, so, the self-calibrated intensity demodulation method is suitable for real-time sound monitoring, such as oil pipeline leakage monitoring, voice monitoring and other occasions.

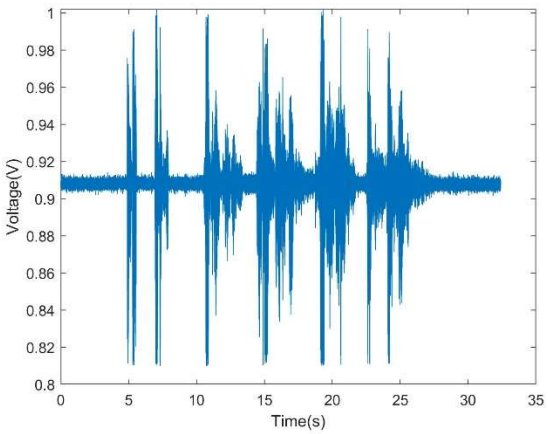

Fig. 8. Acoustic signal demodulated by self-calibrated intensity after noise reduction

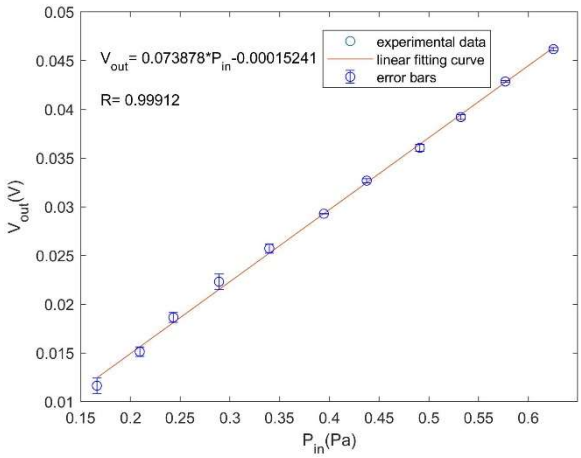

Fig. 9. Acoustic pressure responses of the fiber-optic microphone at 1 kHz.

The voltage sensitivity of the optical fiber microphone was tested at 1 kHz and the sound pressure amplitude P_{in} is gradually increased from 100mPa to 600mPa. The output signals U_{out} of the fiber microphone are shown in Fig.9. The result indicates that there is a good linear relationship between the P_{in} and the U_{out} with a linear correlation coefficient (R) of 0.999. The voltage sensitivity of the fiber microphone can be calculated as in the slope of the linear fit curve, which is 0.073878 V/Pa.

The tested frequency response of the fiber microphone is shown in Fig.10. The incident acoustic frequency varies in the range of 0.1 to 3 kHz. The measured voltage sensitivity (V/Pa) can be converted to phase sensitivity (rad/μPa) by eliminating the effect of the output voltage of PD. The results show that the fiber microphone has a relative flat frequency response between 100 Hz and 3000 Hz. The phase sensitivity at 1kHz is -133.82 dB re 1 rad/μPa . The sensor is suitable for low frequency sound pressure detection.

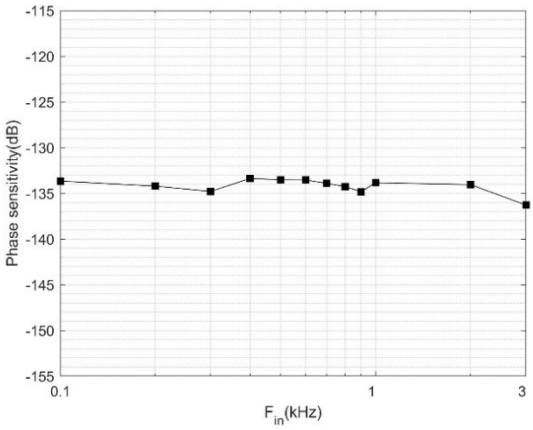

Fig.10. Frequency response of the fiber-optic microphone.

Then, as shown in Fig.11, we established an optic fiber microphone array positioning system which consists of three EFPI acoustic sensors. The distance between adjacent sensors is 10cm, and the sensors are installed in a piece of glass plate of 20cm×30cm. The light from the broadband light source is divided into three paths through 1×3 coupler, and the signal of each sensor is demodulated by self-calibrated intensity demodulation method, received by PD, collected by FPGA, and finally be sent to the upper computer for processing. The coordinates of the three sensors are $(-10\text{cm}, 0\text{cm})$, $(0\text{cm}, 0\text{cm})$ and $(10\text{cm}, 0\text{cm})$, respectively.

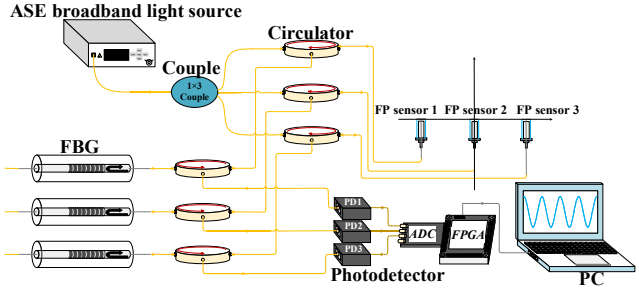

Fig. 11. Block diagram of optical fiber microphone array sound source localization system.

The frequency of sound source is 1 kHz in the experiment and the sampling frequency of the FPGA is 100 kHz. Firstly, the collected signals are noise reduction and normalized, then the effective signals are extracted, and then the time difference is calculated according to (6). The sound source can be located by substituting the time difference into (7). When the coordinate of sound source is $(20\text{cm}, 40\text{cm})$, the typical time-domain waveforms detected by three sensors are shown in Fig.12.

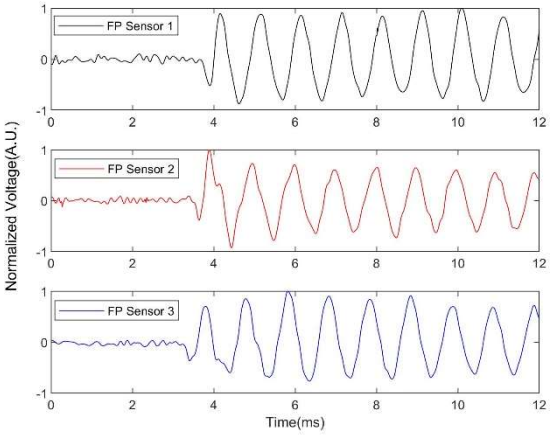

Fig.12. When the coordinate of sound source is $(20\text{cm}, 40\text{cm})$, the typical time domain waveforms detected by three sensor systems are as follows.

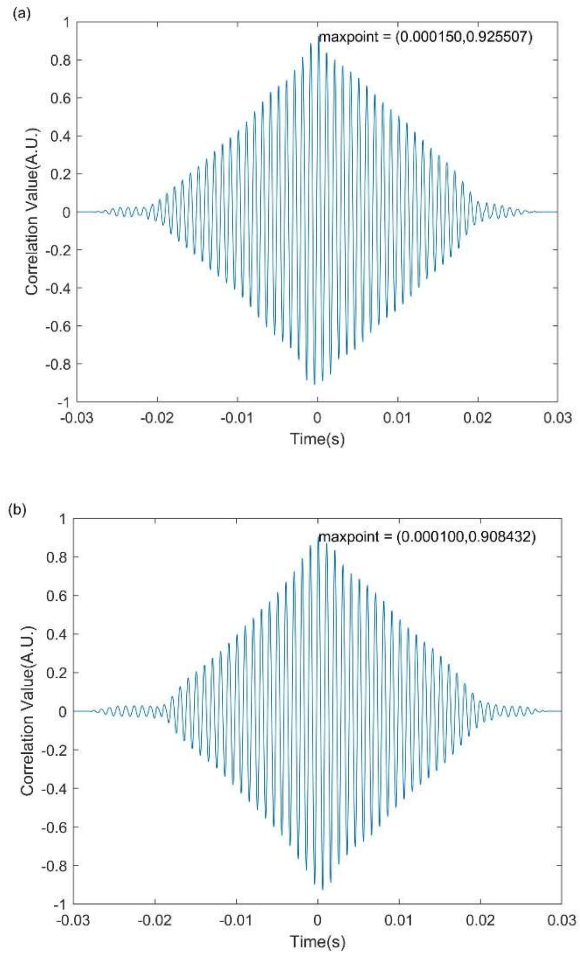

Fig.13. When the coordinate of sound source is $(20\text{cm}, 40\text{cm})$, the time domain correlation of the three sensors was analyzed. (a) The correlation between sensor 1 and sensor 2; (b) Correlation between sensor 2 and sensor 3.

Through autocorrelation operation, the TDOA between FP sensor 1 and FP sensor 2 was calculated as 0.15ms, and the TDOA between FP sensor 2 and FP sensor 3 was calculated as 0.1ms. The correlation function curve is shown in Fig.13. The location results are shown in Table 1. The average positioning error of the system is no larger than 4.82%. Experiments show that the sound source location system with three EFPI sensors can locate the sound source accurately.

Table 1 Results of sound source location

Experiment number	Actual location(cm)		Positioning results(cm)		Positioning error	
	x_0	y_0	x_1	y_1	$\lvert x_1 - x_0\rvert/x_0$	$\lvert y_1 - y_0\rvert/y_0$
1	20	40	20.49	41.62	2.45%	4.05%
2	20	60	20.42	61.4	2.1%	2.33%
3	30	40	27.93	37.39	6.9%	6.53%
4	40	60	36.87	57.21	7.83%	4.65%

Because of the 100 kHz sampling frequency of the signal, the theoretical time delay estimation error may be 0.01ms. We eliminate the variable y from (7), then the total differential of x to τ_{12} and τ_{23} can be expressed as

$$\Delta x = \frac{\partial x}{\partial \tau_{12}}\Delta\tau_{12} + \frac{\partial x}{\partial \tau_{23}}\Delta\tau_{23} \tag{8}$$

The minimum values of $\Delta\tau_{12}$ and $\Delta\tau_{23}$ are determined by the sampling rate. The higher the sampling rate, the higher the positioning accuracy. Therefore, it is possible to improve the positioning accuracy by increasing the sampling rate.

When the coordinate of sound source is $(20\text{cm}, 40\text{cm})$, the theoretical TDOA (τ_{12}, τ_{23}) is $(1.52181 \times 10^{-4}\text{s}, 1.00624 \times 10^{-4}\text{s})$, the TDOA (τ'_{12}, τ'_{23}) calculated by the correlation function is $(1.5 \times 10^{-4}\text{s}, 1 \times 10^{-4}\text{s})$, therefore $(\Delta\tau_{12}, \Delta\tau_{23})$ is $(-2.181 \times 10^{-6}, -6.24 \times 10^{-7})$. The $\left(\frac{\partial x}{\partial \tau_{12}}, \frac{\partial x}{\partial \tau_{23}}\right)$ is $(-3.3849 \times 10^{5}\text{cm/s}, 4.2214 \times 10^{5}\text{cm/s})$. By substituting $(\Delta\tau_{12}, \Delta\tau_{23})$ and $\left(\frac{\partial x}{\partial \tau_{12}}, \frac{\partial x}{\partial \tau_{23}}\right)$ into (8), we can obtain the $\Delta x = 0.4748\text{cm}$, this value is close to the positioning error of the actual system.

The comparisons between the system performance in this paper and that in the literature are shown in Table 2. It must be noted that considering that the positioning accuracy of the left and right sensors in this system is the same, so, the distance in the direction of the sensor is actually 2×40cm. Therefore, the actual measurement spatial range of this paper is 80cm×60cm.

Table 2 The comparison of the system performance in this paper between that in the literature

	Technology	Complexity	Cost	Positioning accuracy	Spatial range
Ref.8	EFPI	high	high	3.55cm	60cm×60cm
Ref.10	EFPI	low	high	5.14cm	100cm×100cm×100 cm
Ref.11	Φ-OTDR	high	high	2.49cm	50cm×40cm×30cm
This paper	EFPI	low	low	3.13cm	80cm×60cm

4. Conclusion

A two-dimensional sound source localization system based on fiber FP cavity microphone array is successfully realized. The self-calibrated intensity demodulation scheme is used to demodulate the sound signal, and the starting point and end point of the sound are found out through the signal extraction technology, and then the TDOA of the two signals is calculated through the cross-correlation algorithm. Finally, the position of the sound source can be calculated by substituting the geometric positioning algorithm. The average positioning error of the system is no larger than 4.82%, which proves the effectiveness of the system. The system has the advantages of simple structure, high positioning accuracy and low cost. It has high engineering application value in voice monitoring.

Acknowledgement

This work was supported in part by the Natural Science Foundation of Jiangxi Province under Grant 20202ACBL202002, in part by The Academic and Technical Leader Plan of Jiangxi Provincial Major Disciplines under Grant 20172BCB22012, in part by the National Natural Science Foundation of China under Grant 61465009.

References

1. G.Y.Li, Z.D.Guo, and S.L.Chen, “Miniature probe for forward-view wide-field optical-resolutin photoacoustic endoscopy,” IEEE Sensors Journal, vol.19, no.3, pp.909-916, 2019.
2. B.Fischer, “Optical microphone hears ultrasound,” Nature Photonics, vol.10, no.6, pp.356-358, 2016.
3. M.Eriksrud, J.Langhammer, and H.Nakstad, “Towards the optical oilfield,” Houstion :SEG Houston International Exposition and Annual Meeting, 2009.
4. S.Preisser, W.Rohringer, M.Y.Liu, R.Haindl, and W.Drexler, “All-optical highly sensitive akinetic sensor for ultrasound detection and photoacoustic imaging,” Biomedical Optics Express, vol.7, no.10, pp.4171–4186, 2016.
5. K.Chen, M.Guo, S.Liu, B.Zhang, H.Deng, Y.Zheng, Y.Chen, C.Luo, L.Tao, M.Lou, and Q.Yu, “Fiber-optic photoacoustic sensor for remote monitoring of gas micro-leakage,” Optics express, vol.27, no.4, pp.4648-4659, 2019.
6. C.Nian, X.Li, and W.Ying, “Multiplexing of anti-resonant reflecting optical waveguides for temperature sensing based on quartz capillary,” Optics Express, vol.26, no.25, pp.33501-33509, 2018.
7. P.Wei, X.L.Han, and D.Xia, “Measurement method for the velocity of acoustic emission wave in liquid nitrogen,” IEEE Transactions on Industrial Electronics, vol.65, no.10, pp.8232-8238, 2018.
8. J.Y.WANG, F Ai, Q.Z.Sun, T.Liu, H.Li, Z.J.Yan, and D.M.Liu. “Diaphram-based optical fiber sensor array for multipoint acoustic detection,” Optics Express, vol.26, no.19, pp.25293-25304, 2018.
9. Q.Liu, Z.G.Jing, A.Li, Z.Xia, and W.Peng, “Multiplexing fiber-optic Fabry-Perot acoustic sensors using self-calibrating wavelength shifting interferometry,” Optics Express, vol.27, no.26, pp.38191-38203, 2019.
10. S.E.Hayber and S.Keser. “3D sound source localization with fiber optic sensor array based on genetic algorithm,” Optical Fiber Technology. 57 (2020) 10229.
11. Z.C.Liu, L.Zhang, H.M.Wei, Z.L.Xiao, Z.H.Qiu, R.Q.Sun, F.F.Pang and T.Y.Wang. “Underwater acoustic source localization based on phase-sensitive optical time domain reflectometry,” Optics Express, vol.29, no.9, pp.12880-12892, 2021.
12. J.Wang, H.Peng, P.Zhou, J.Guo, B.Jia, and H.Wu, “Sound source localization based on Michelson fiber optic interferometer array,” Optical Fiber Technology, vol.51, no.4, pp.112-117, 2019.
13. V.S.Lavrov, M.Y.Plotnikov,S.M.Aksarin, M.E.Efimov, V.A.Shulepov, A.V.Kulikov, and A.U.Kireenkov, “Experimental investigation of the thin fiber-optic hydrophone array based on fiber Bragg gratings,” Optical Fiber Technology, vol.34, pp.47-51, 2017.
14. X.Mao, S.Yuan, X.Wang, and P.Zheng, “Stabilized fiber-optic Fabry-Perot acoustic sensor based on improved wavelength tuning technique[J]. Journal of Lightwave Technology, vol.35, no.11, pp.2311-2314, 2017.
15. A.Dandridge, A.B.Tveten, and T.G.Giallorenzi, “Homodyne Demodulation Scheme for Fiber Op-ticSensors Using Phase Generated Carrier,” IEEE Transactions on Microwave Theory andTechniques, vol.30, no.10, pp.1635-1641,1982.
16. G.Zhang, Q.Yu, and S.Song, “An investigation of interference/intensity demodulated fiber-optic Fabry-Perot cavity sensor,” Sensors and Actuator A:Physical, vol.116, no.1, pp.33-38, 2004.
17. Y.Wu, C.Yu, F.Wu, C.Li, J.Zhou, Y.Gong, Y.Rao, and Y.Chen, “A highly sensitive fiber-optic microphone based on graphene oxide membrane,” Journal of Lightwave Technology, vol.35, no.19, pp.4344-4349, 2017.
18. A.Wang, H.Xiao, J.Wang, Z.Wang, W,Zhao, and R.G.May, “Self-Calibrated interferometric/intensity based optical fiber sensors,” Journal of Lightwave Technology, vol.19, no.10, pp.1495-1501, 2001.
19. F.Guo, T.Fink, M.Han, L.Koester, J.Turner, and J.Huang, “High-sensitivity, high-frequency extrinsic Fabry-Perot interferometric

fiber-tip sensor based on a thin silver diaphragm," Optics Letters, vol.37, no.9, pp.1505-1507, 2012.

20. J.L.Chen, J.Z.Wang, and T.Y. Sun, "A multiplanes geometric approach for sound source localization with TDOA," International Conference on System Science and Engineering. New Taipei, Taiwan, China:IEEE, 2018:1-5.